Detecting and Avoiding Gap-Like Structures on a Variable-Sweep Wing UAS

John Schmidt, Frank Cianciarulo, Graham Buccheri
Norman Wereley, Huan Xu

***Abstract*— We present the design and testing of an uncrewed aerial system (UAS) for obstacle avoidance of gap-like structures at high speed. Prior work in fixed-wing UAS obstacle avoidance has shown success at high speeds for going around obstacles, while going through obstacles is limited to low speeds and mainly accomplished by rotary-wing UAS. There exists a need for UAS to retain high speed obstacle avoidance using both go-around and go-through maneuvers. To address that need, we designed and tested a hardware-in-the-loop (HITL) implementation of a novel sweeping wing mechanism that decreases the effective wingspan of our aircraft and enables flight through small spaces; we also proposed a decision making algorithm based on the HITL tests that enables both go-around and go-through behavior. The sweeping wing mechanism uses a pneumatic artificial muscle (PAM) and 3D printed components, and it was designed specifically for a stock radio-controlled aircraft that can reach top speeds of over 53 m/s. Although prior work into novel dynamic structures for UAS has been done, none of these structures have been used for flying through gap-like structures. Our HITL tests suggest that our platform can perform go-through maneuvers at speeds up to 25 m/s, which is considerably faster than the top speeds tested in prior work. However, our obstacle detection and avoidance algorithms were greatly simplified, meaning that our data would only be valid under ideal conditions.**

I. Introduction

Flying uncrewed aerial systems (UAS) in obstacle dense environments is a difficult obstacle avoidance problem. For example, flying through a wooded area poses a threat to UAS because of potential collisions with trees. Obstacle avoidance methods used on fixed-wing UAS mainly involve aggressive acrobatic and go-around maneuvers. Unlike rotary-wing UAS, fixed-wing UAS cannot stop mid-flight and hover, and they have to sustain higher speeds to remain in flight. Because of this, fixed-wing platforms are usually constrained by their physics to make these dramatic avoidance maneuvers when avoiding obstacles. Rotary-wing UAS such as quadrotors, on the other hand, lack the speed and flight endurance of similarly sized fixed-wing UAS. What quadrotors lack in speed and endurance, they make up for in agility and hover capabilities, allowing them to perform go-through maneuvers to clear gap-like structures, such as spaces between tree branches or open windows in an urban environment. This project aims to bridge the gap between the obstacle avoidance methods available to fixed-wing and rotary-wing UAS. We did this by developing a UAS platform that avoids gap-like obstacles with go-through maneuvers while still retaining high speed go-around behavior. By implementing a mechanism that varies the wing sweep angle, we believe that we can achieve the ability to go-through and go-around gap-like structures at high speeds on a fixed-wing UAS.

Mechanisms that modify the physical structure of a fixed-wing UAS and its aerodynamics have been studied and used for various purposes. Mechanisms that sweep the wings of the UAS, in particular, already exist. In larger manned aircraft like the U.S. Navy's F-14 Tomcat, the purpose of sweeping the wings backwards is to reduce and mitigate the high drag and structural loads associated with flying at high Mach numbers. However, for autonomously flown UAS, sweeping wing mechanisms have recently been used for other purposes. Fletcher et al. have worked on varying the sweep angle in tandem with thrust and elevator deflection in order to achieve controlled perched landings in various headwinds, with airspeeds topping out at 15 m/s [1]. Maldonado et al. have also worked on controlled perched landings for autonomous UAS in recent years, except they used an ornithoper as opposed to a traditional fixed-wing aircraft with sweeping wings [2]. An ornithoper produces lift and thrust by flapping its wings, mimicking the motion of flying wildlife like bats, birds, and insects. Other recent work on ornithoper technology has involved active obstacle detection and avoidance, particularly that done by Rodríguez-Gómez et al. [3]. Their ornithopter platform was able to detect and avoid moving obstacles at relative speeds up to 11 m/s. Research done by Pérez-Cutiño et al. and Ruiz et al. has led to improvements in autonomous flight control of ornithopers via trajectory optimization and better understandings of their aerodynamics [4] [5]. Rosen et al. also worked on a flapping-wing aerial system, but on the insect-scale with the purpose of studying flight control schemes at such a small scale [6]. Other notable dynamic structure work includes that by Communier et al. and Bashir et al., with both groups working on morphing leading and trailing edges of their wings to improve aerodynamic performance [7] [8] [9]. To the best of our knowledge, none of the mechanisms in these platforms have been used for obstacle avoidance of gap-like structures, and sweeping wing technology has not yet been used for obstacle avoidance at all.

The majority of work on fixed-wing obstacle avoidance leverages improvements in detection algorithms and computationally efficient control strategies to enable aggressive and acrobatic maneuvers, rather than relying on novel dynamic structures. For example, work done by Beyeler et al. and

*This project was tasked by the Army Research Labs as part of the development of an impact resistant variable-sweep wing UAS, with an emphasis on active obstacle avoidance.

by Barry et al. demonstrated platforms flying and avoiding obstacles at speeds of 14 m/s with the use of novel methods of obstacle detection [10] [11]. In particular, Beyeler et al. used a form of optic flow while Barry et al. developed a novel form of pushbroom stereo to improve detection times and aircraft reaction speed. However, Barry et al. used a limited trajectory library that involved banked turns to go-around obstacles. Bulka and Nahon worked on an improved trajectory library that included more aggressive and aerobatic maneuvers for autonomous fixed-wing UAS obstacle avoidance, but they compromised on flight speed with simulated aircraft flying at 7 m/s [12]. Keshmiri et al. have also demonstrated high speed collision avoidance between large fixed-wing UAVs at speeds of 18 m/s in flight tests, although the position and velocity of the UAV acting as an obstacle was shared between aircraft [13]. Adhikari and de Ruiter, Kahagh et al., and Lin et al. also worked on fixed wing obstacle avoidance with results shown in simulation [14] [15] [16]. In each of these attempts to solve the problem of high speed obstacle avoidance for fixed-wing UAS, the method involves some sort of go-around behavior, not go-through behavior.

Existing obstacle avoidance research focused on flying through gaps has mainly been limited to rotary-wing UAS. For example, Sanket et al. developed an algorithm for detecting gaps of any shape, as opposed to rectangular windows, with tolerances of 5 cm [17]. Their hardware implementations tested quite slow, however, flying around 2-3 m/s. Jiang et al. also worked on flying quadrotors between stands of trees, but their results always showed at least 1.38 m of clearance between their UAS and their obstacles [18]. Zhao et al. developed a novel deformable rotary-wing UAS, which would aid in passing through narrow spaces, although most of their work was focused on characterizing their system's kinematics [19]. Despite the high speed nature of fixed-wing aircraft, Barry et al. made an effort of achieving obstacle avoidance via go-through maneuvers [20]. In particular, they performed this feat with a knife-edge maneuver, which is a maneuver in which the aircraft flies forward with one wingtip pointing toward the ground and the other wingtip pointing toward the sky. They claimed to have flown at 7 m/s between gaps slightly smaller than the wingspan of their aircraft. Barry et al.'s results on go-through obstacle avoidance were only able to reach half the speed achieved by their go-around methods listed earlier. The ability to go-through obstacles appears to come at the cost of speed for both conventional rotary-wing and fixed-wing UAS.

The contributions of this paper are:
I: The development of a novel sweeping wing mechanism for fixed-wing UAS go-through obstacle avoidance,
II: The implementation and validation of our sweeping wing mechanism in hardware-in-the-loop (HITL) tests at different airspeeds, and
III: The design of a go-around vs go-through decision making algorithm informed by the results of the HITL tests that lets our fixed-wing platform retain high speed go-around behavior.

The remainder of this paper is structured as follows: Section II goes over the hardware designs involved in modifying a stock radio-controlled (RC) aircraft to meet our goals. This includes a description of the added components that enabled autonomous flight and a description of the novel sweeping wing mechanism. Section III discusses the experimental design for the HITL testing of our platform. This section also touches on our obstacle detection and avoidance algorithms. Section IV details both the results from our HITL tests and a refinement of our avoidance algorithm, while Section V summarizes the work done and brings up future considerations.

II. Platform Design

Figure 1 shows the base platform that we used throughout this project: the Horizon Hobby E-flite V900. The V900 is a radio-controlled fixed-wing aircraft with a wingspan of 0.899 m (35.4 in), a weight of 0.840 kg (1.86 lbs), and a top speed of over 53 m/s (120 mph) out of the box when paired with a 4S LiPo battery. The base V900 has no autonomous capabilities as it carries a receiver inside its fuselage that only takes commands from a manual transmitter. The aircraft has a conventional flight control surface configuration, with two ailerons, an elevator, a rudder, and throttle control.

Fig. 1. The original, unmodified aircraft that was used in this project is a sleek and fast RC airplane made for flight at airspeeds of over 53 m/s (120 mph).

A. Autonomous Flight Hardware

We added additional hardware to the V900 to enable autonomous flight capabilities. A GPS and pitot-static system gather state information on the aircraft such as position and airspeed. Both sensors came from mRobotics. We mounted the pitot tube from the pitot-static system far enough away from the root of the left wing so that the downwash from the propeller would not interfere with airspeed measurements. A special 3D printed canopy replaced the original foam canopy on the fuselage in order to house the GPS as close as possible to the center of mass of the aircraft.

We also added an ArduPilot based flight controller to take in the state information from the above sensors and feed

it back to a ground control station (GCS) running on an external PC via a telemetry radio. We used MissionPlanner as the GCS in this project; trajectory and flight control surface commands could also be sent back to the V900 from the GCS to enable autonomous flight. This flight controller also acted as a middleman between the RC receiver and the output flight control surfaces so that we could still operate the V900 manually with an RC transmitter. Once again, the flight controller and telemetry radio came from mRobotics. As for mounting, we wedged the flight controller into the fuselage where the original receiver was located, and we draped the telemetry radio's antenna along the side of the fuselage near the right wing root to help with balancing the roll moment from the pitot tube. We also added metallic washers on the underside of each wing root to further balance the weight and moments on the aircraft.

A camera is the last piece of hardware that was required for autonomous flight on the V900. A camera would send video of what is in front of the V900's flight path back to the GCS and PC via the flight controller and telemetry radio. Obstacle detection and avoidance software running on the PC would then process the video stream and allow the aircraft to perform its go-around vs go-through decision making behavior. The camera must face in the same direction as the nose of the V900, placed on top of the fuselage.

B. Novel Sweeping Wing Mechanism

The design of the sweeping wing mechanism can be split into two parts: the gear mechanism used to sweep the wings, and the actuation device used to actuate the gear system. In brief, the actuation device retracts the wings when pressurized; when it is depressurized, a spring restores the wings to their original degree of sweep.

1) Gear Mechanism: We made a 3D scan of both the wing and the fuselage of the V900 to generate 3D models to use as a basis for designing the mechanism and housing. The system was mostly made of soft components and 3D printed plastics to reduce weight. To construct the mechanism, a wing mount was designed to match the leading edge of the wing from the scan. This mounting piece was then connected to a shaft with a one-inch diameter gear at the end. This gear then met with a quarter inch diameter gear, creating a 4:1 gear ratio. The quarter inch diameter gear then met with a linear gear. The linear gear was attached to the actuation system and spring. This gear system was mirrored for the opposite wing, making use of the same linear gear for both wings. When actuated, the linear gear would slide aft, turning the quarter inch diameter gear, which in turn rotated the one-inch diameter gear and wing.

2) Actuation Device: A 7/8-inch diameter pneumatic artificial muscle (PAM) with 3D printed end fittings was used for actuation. A PAM is an actuator comprised of a latex bladder in a Kevlar sheath. The bladder and braid are held together by use of an end fitting. 3D printed end fittings were desired to reduce the weight of the system, as opposed to the typical aluminum end fitting. The total mass of the assembled PAM used in the mechanism was 0.258 kg (0.57 lbs). When inflated with a working fluid such as air, PAMs contract axially and produce an axial force. By placing the PAM in line with the linear gear, the PAM is able to pull the gear to retract the wings. A small metallic spring is placed on the opposite end of the gear, which aids to pull the gear back into its original position when the PAM is deflated. The sweeping wing mechanism can be seen in Figure 2.

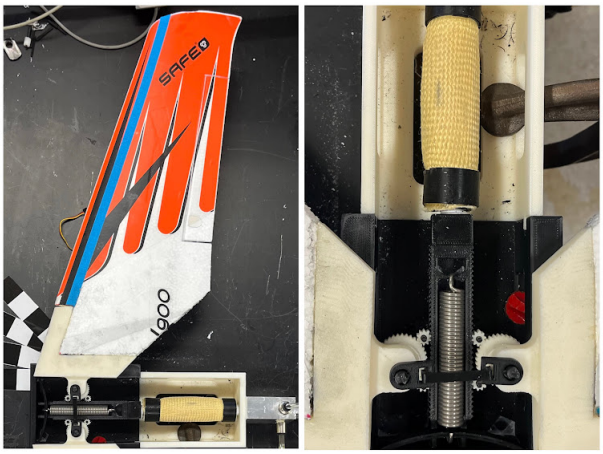

Fig. 2. Left: The sweeping wing mechanism is shown with one wing attached. Right: The white PAM that actuates the mechanism, the restoring spring, and the gear mechanism are housed in a 3D printed structure that is meant to fit under the fuselage of the V900.

All these components are shown in the system diagram in Figure 3, and a physical depiction of the autonomous V900 minus the camera and sweeping wing mechanism is shown in Figure 4.

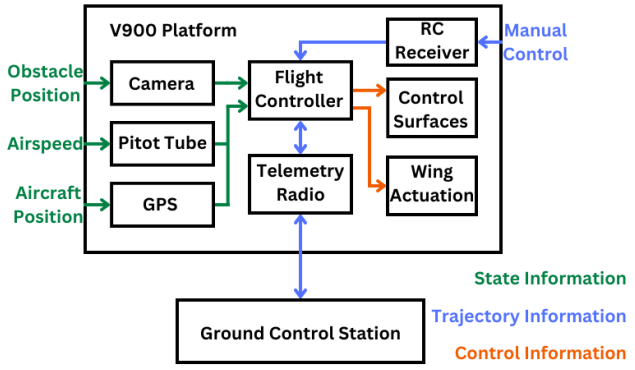

Fig. 3. System diagram of the autonomous flight enabled V900 showing the flow of state information from the sensors, trajectory and flight control data from the transmitter and GCS, and raw output signals to the control surfaces.

III. Experimental Design

We first attempted true flight tests with the modified V900 in Figure 4 by autonomously flying circles around a point. From these flight tests, we were able to establish just over 13 m/s (30 mph) as the minimum airspeed required for flight. The V900 also briefly held 27 m/s (60 mph), which we will use as a benchmark for cruise speed going

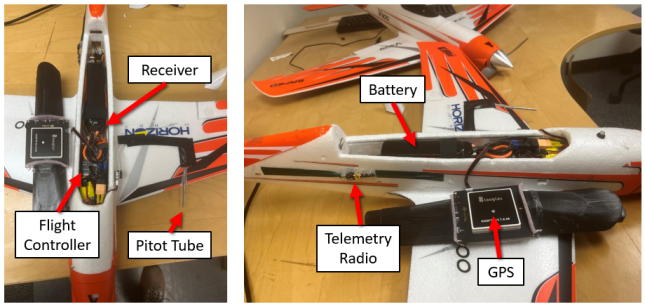

Fig. 4. Left: Top down view of the fuselage section of the modified V900. Right: Side view of the same section. The 3D printed canopy with the GPS is popped off, the pitot tube is channeled through the left wing, the telemetry radio is draped along the right hand side of the fuselage, and all the remaining components minus the camera and sweeping wing mechanism are packed into the fuselage. This aircraft weighed 0.235 kg (0.52 lbs) more than the base V900.

forward. Considering adding the weight of a camera and the sweeping wing mechanism (0.258 kg), the envisioned final platform would prove risky to fly. Instead of taking on these risks to our equipment, we opted for a safer HITL test approach. Instead of flying the actual aircraft, our tests fed pre-recorded footage of "flying" toward an obstacle into the GCS and PC. The GCS and PC would then run our obstacle detection software, sending a signal activating the sweeping wing mechanism (separate from the rest of the aircraft) if an obstacle was detected, as shown in Figure 5. To enable go-around behavior, we also developed an early version of our decision making algorithm, which we graphically depicted with a simulated flight path in the GCS, shown in Figure 6. We will now go into the specifics of how our obstacle detection and avoidance software works.

A. *Obstacle Detection and Avoidance*

We begin this section by defining what our obstacles are. Ideally, we want our UAS to be able to fly through any gap-like structure, such as spaces between tree branches or flag poles, or even through open windows. However, since the main contribution of this work is focused on proving the sweeping wing mechanism as a viable method of high speed go-through obstacle avoidance, we simplified obstacle detection to detection of an Aruco tag. Aruco tags are square markers that have pre-existing obstacle detection libraries available in Python, and detection can be accomplished by any single camera. By placing Aruco tags in our pre-recorded videos, we were able to simulate flying toward a rectangular window. As soon as the Aruco tag / obstacle is detected by a program running on the PC, the sweeping wing mechanism is activated. Since the sweeping wing mechanism was separate from our modified V900 in our HITL tests, we used an Arduino board to assume the role of the flight controller and take a signal from the PC and control the wing sweep.

As with any obstacle detection algorithm, the Aruco tag detection we used cannot see the obstacle from infinitely far away. Our tag detection program could only see 0.10 m (4 in) width tags up to 1.8 m (6 ft) away when using a phone

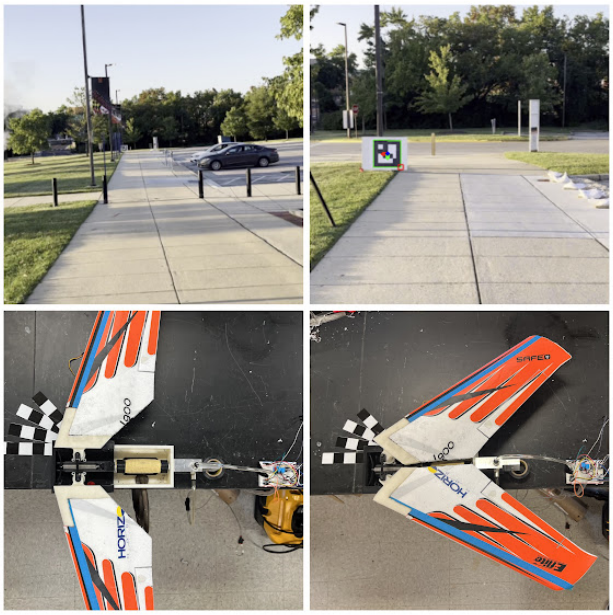

Fig. 5. Top Left: No Aruco tag is detected. Top Right: An Aruco tag is detected; Flight path is assumed toward the center of the obstacle. Bottom Left: Wings are in the normal configuration. Bottom Right: Wings are fully swept back.

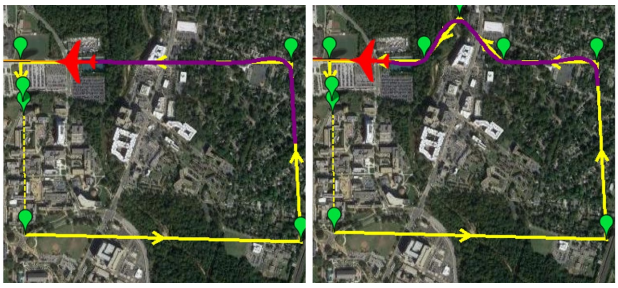

Fig. 6. Left: A fixed-wing UAS completes the last leg of its simulated flight path in the GCS. Right: An obstacle on the last leg of the flight path forces a go-around decision, dynamically changing the flight path mid-flight. The flight path is marked by yellow vectors pointing toward green waypoints, and the path followed by the UAS is marked in purple.

camera in a dimly lit room, but we found that the maximum detection distance scaled linearly with the width of the Aruco tag. Assuming a cruise speed v of about 27 m/s (60 mph) and an early 0.5 s estimate of the time t_r needed to retract the wings fully, we calculated that the UAS needs to detect an obstacle at least 13 m (44 ft) away. Using 13 m as the smallest detection distance d to see an obstacle to enable a full sweep of the wings, we would need Aruco tags with a width of at least 0.76 m (30 in). In other words, if our V900 was flying at an airspeed of 27 m/s and saw an Aruco tag any smaller than 0.76 m, it would not be able to fully sweep its wings in time to go through the gap, theoretically.

We used two maneuvers for obstacle avoidance. The first is the go-through maneuver, which only involves sweeping the wings of the V900 far enough back that the effective wingspan is smaller than the width of the obstacle. The second is the go-around maneuver, which is visualized on

the GCS as a deviation from and then return to the original flight path. Specifically, a Python program runs on the GCS and PC that dynamically adds new waypoints to the original flight path in the case of a go-around. The GCS would then command the UAS via the flight controller to go-around using coordinated turns. The go-around decision is made if the obstacle is detected with less time than that required for a full sweep of the wings. This decision making algorithm is shown in pseudocode in Algorithm 1. To further simplify our obstacle avoidance methods, we assumed that the UAS has no altitude loss during the duration of the flight, and that our UAS flies straight and level toward the Aruco Tag.

Algorithm 1 Go-Around vs Go-Through V.1

```
t_r = 0.5s time required to fully retract wings
d = 13m distance at which obstacle is detected
v = airspeed at which obstacle is flying
while searching for obstacle and on course do
    if obstacle in sight then
        calculate t_2o = d/v time left before obstacle is reached
        if t_2o < t_r then
            create new waypoint and go-around
        else
            sweep wings back and go-through
        end if
    end if
end while
```

Initially, we used 0.5 s as an estimate for t_r and 13 m as an estimate for d in Algorithm 1. With these parameter values under ideal conditions, the UAS would perform go-through maneuvers up to 27 m/s for obstacles of 0.76 m in width.

B. Experimental Goals

To validate the efficacy of our sweeping wing mechanism at go-through obstacle avoidance, we performed HITL tests at various airspeeds. In particular, by measuring the degree of wing sweep reached at different airspeeds, we were able to measure how small the effective wingspan of the V900 became. We were able to simulate flying at different airspeeds by speeding up our pre-recorded videos. Our videos were also taken on a phone camera outside in a well lit environment while trying to hold a constant speed on a bicycle with a speedometer. Because of this, $d = 13$ m was not necessarily true. We also recorded values of t_r at various PAM pressures, and we found t_r to be greater than the initial estimate of 0.5 s. From these results, we modified the go-around vs go-through decision making algorithm. We will discuss the results of our HITL tests in the next section.

IV. Discussion

We first measured t_r at pressures ranging from 55 to 85 PSI, with results shown in Figure 7. We found that the optimal PAM pressure for testing our sweeping wing mechanism at different airspeeds was 85 PSI, with $t_r \approx 1.4$ s. This is significantly longer than our initial estimate of 0.5 s, which was conjectured before the actual sweeping wing hardware was implemented. Regardless, we continued the remainder of our tests with holding the PAM pressure at 85 PSI.

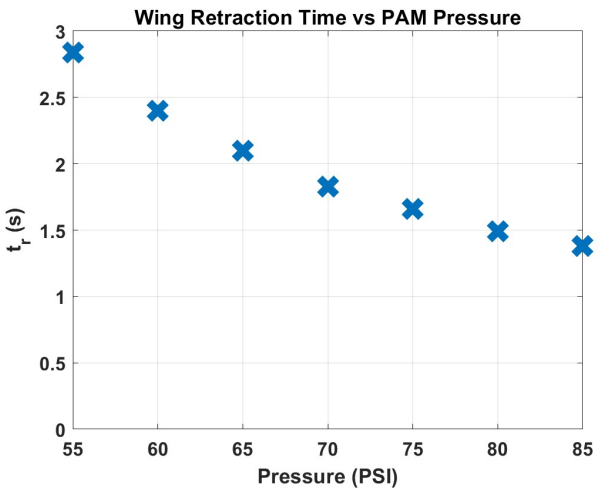

Fig. 7. The time required to fully retract the wings t_r is shown to decrease as PAM pressures increase. The PAM pressure was not allowed to go above 85 PSI as a safety requirement.

We next confirmed that no sweep (0 degrees) corresponds to the normal 0.899 m (35.4 in) wingspan, and then we measured the fully swept back wingspan (37 degrees) to be 0.610 m (24.0 in). From this, we fit a sinusoidal function to relate the degree of wing sweep θ to the effective wingspan l_e:

$$l_e = \frac{1}{39.37}(60.6\cos\theta - 23.6) \tag{1}$$

A sinusoidal function is appropriate since the sweeping wing mechanism acts by pivoting each wing about a point, which makes the wingtips trace a circular arc when retracting.

Using Equation 1 we found the effective wingspan and thus smallest obstacle width that can be cleared with a go-through maneuver at airspeeds ranging from about 5-45 m/s (10-100 mph). This data is shown in Figure 8. Due to airspeed requirements necessary to keep the V900 flying, only airspeeds above 13 m/s (30 mph) are viable, with unviable airspeeds below marked in blue. The range of airspeeds from 13-18 m/s (30-40 mph) allow for a full sweep of the wings, which are marked in green. The range of airspeeds marked in orange from 18-25 m/s (40-55 mph) do not allow for a full retraction of the wings, but are still viable in our particular HITL tests because the smallest clearable obstacle width remains below 0.76 (30 in), which is the actual obstacle width or Aruco tag size used in our videos. At speeds above 25 m/s, we can no longer avoid our obstacle with a go-through maneuver, and no fixed-wing UAS obstacle avoidance algorithm has proven successful at go-around maneuvers at these high speeds. For that reason, flying in this red range of airspeeds will likely result in a collision if an obstacle is encountered. It is also important to point out that as the aircraft approaches its top speeds

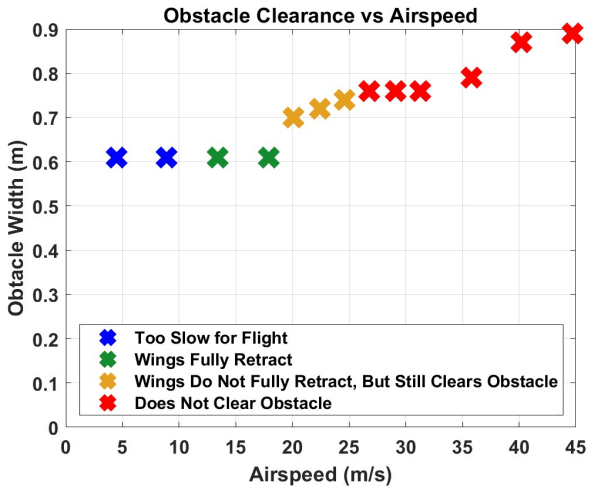

Fig. 8. The smallest obstacle width that can be cleared with a go-through maneuver is shown at various airspeeds. Only the range of airspeeds from 13 m/s to 25 m/s are viable (green and orange points).

of over 45 m/s (100 mph), that the effective wingspan also approaches the normal wingspan of about 0.9 m.

Algorithm 2 Go-Around vs Go-Through V.2

$t_r = 1.4s$ time required to fully retract wings
$v =$ airspeed at which obstacle is flying
$l_{e,min} = 0.61m$ smallest effective wingspan possible
$l_{e,worst} = 0.76m$ worst case effective wingspan, 25 m/s
while searching for obstacle and on course **do**
  if obstacle in sight **then**
    calculate $d =$ distance at which obstacle is detected
    calculate $w =$ width of obstacle
    calculate $t_2o = d/v$ time left before obstacle is reached
    if $v < 18m/s$ **then**
      if $t_2o < t_r$ OR $w < l_{e,min}$ **then**
        create new waypoint and go-around
      else
        sweep wings back and go-through
      end if
    else if $18m/s < v < 25m/s$ **then**
      if $w < l_{e,worst}$ **then**
        create new waypoint and go-around
      else
        sweep wings back and go-through
      end if
    else
      speed too high, crash likely
    end if
  end if
end while

Note that although our actual t_r was almost 3 times greater than our initial estimate, we can still clear our obstacles with go-through maneuvers at 25 m/s, which is just 2 m/s below our initial airspeed limit of 27 m/s. This suggests that we are actually detecting our obstacles in the pre-recorded videos at distances greater than $d = 13$ m. This is likely due to external factors in the pre-recorded videos such as lighting affecting how well the camera is able to resolve the Aruco tag. Because of the variability in d and the higher than expected t_r value not allowing for full wing sweep at speeds of 18-25 m/s, our decision making algorithm had to be refined, as shown in Algorithm 2.

In Algorithm 1, we held d constant and assumed a known obstacle width; whereas in Algorithm 2, we calculate these values upon an obstacle detection. The Python libraries for Aruco tag detection can make these calculations as long as the camera being used is calibrated properly. We also changed the go-around vs go-through criteria depending on which range of airspeeds the aircraft happens to be flying at. At lower airspeeds, if there is not enough time for a full sweep or if the obstacle width is too small, then the UAS will go-around. At higher airspeeds, the criteria for what makes an obstacle too small changes based on findings from Figure 8, while time is ignored since the UAS will not be able to retract its wings fully at these speeds. In particular, we use the worst case effective wingspan found at 25 m/s as the obstacle width limit.

V. Conclusion

In HITL tests, our UAS platform was able to clear our obstacle with go-through maneuvers up to 25 m/s, which is well above the 18 m/s benchmark for fixed-wing UAS obstacle avoidance found in prior work. However, our setup was simplified greatly with assumptions that placed our UAS perfectly tracking and flying towards the obstacle in the case of go-through maneuvers. Our obstacle detection and avoidance algorithms were also simplified, using Aruco tags as proxies for gap-like structures and only coordinated turns as go-around maneuvers. Results from our HITL tests helped refine our go-around vs go-through decision making algorithm; however, a more thorough testing of the decision making algorithm would be helpful in validating go-around abilities of the platform.

Future considerations would first include the design of a custom platform that is more stable in flight and has a higher weight capacity than that of the V900. This would allow us to move from HITL tests to true flight tests. However, altitude loss from wing sweep induced droop, imprecise trajectory control from faulty sensors, and position drift from wind would have to be accounted for. We also desire to extend our Aruco tag detection to more advanced obstacle detection methods, perhaps substituting solutions from prior work for true gap detection. Finally, improvements to the novel sweeping wing mechanism could be made to safely increase the PAM pressure level and lead to a lower t_r.

Acknowledgement

A special thanks to Aditi Ramadwar for her help on the Aruco tag detection code used in this project.

REFERENCES

[1] Liam J. Fletcher, Robert J. Clarke, Thomas S. Richardson and Mark Hansen. "Integrating Throttle into a Reinforcement Learning Controller for a Perched Landing of a Variable Sweep Wing UAS," AIAA 2022-1288. AIAA SCITECH 2022 Forum. January 2022.

[2] F. J. Maldonado, J. Á. Acosta, J. Tormo-Barbero, P. Grau, M. M. Guzmán and A. Ollero, "Adaptive Nonlinear Control For Perching of a Bioinspired Ornithopter," 2020 IEEE/RSJ International Conference on Intelligent Robots and Systems (IROS), Las Vegas, NV, USA, 2020, pp. 1385-1390, doi: 10.1109/IROS45743.2020.9341793.

[3] J. P. Rodríguez-Gómez, R. Tapia, M. d. M. G. Garcia, J. R. M. -d. Dios and A. Ollero, "Free as a Bird: Event-Based Dynamic Sense-and-Avoid for Ornithopter Robot Flight," in IEEE Robotics and Automation Letters, vol. 7, no. 2, pp. 5413-5420, April 2022, doi: 10.1109/LRA.2022.3153904.

[4] Pérez-Cutiño, M.A., Rodríguez, F., Pascual, L.D. et al. Ornithopter Trajectory Optimization with Neural Networks and Random Forest. J Intell Robot Syst 105, 17 (2022). https://doi.org/10.1007/s10846-022-01612-5

[5] Ruiz, C., J. Á. Acosta, and A. Ollero. "Aerodynamic reduced-order Volterra model of an ornithopter under high-amplitude flapping." Aerospace Science and Technology 121 (2022): 107331.

[6] M. H. Rosen, G. le Pivain, R. Sahai, N. T. Jafferis and R. J. Wood, "Development of a 3.2g untethered flapping-wing platform for flight energetics and control experiments," 2016 IEEE International Conference on Robotics and Automation (ICRA), Stockholm, Sweden, 2016, pp. 3227-3233, doi: 10.1109/ICRA.2016.7487492.

[7] Communier D, Botez RM, Wong T. Design and Validation of a New Morphing Camber System by Testing in the Price—Païdoussis Subsonic Wind Tunnel. Aerospace. 2020; 7(3):23. https://doi.org/10.3390/aerospace7030023

[8] Bashir M, Longtin-Martel S, Botez RM, Wong T. Aerodynamic Design Optimization of a Morphing Leading Edge and Trailing Edge Airfoil–Application on the UAS-S45. Applied Sciences. 2021; 11(4):1664. https://doi.org/10.3390/app11041664

[9] Bashir M, Longtin-Martel S, Zonzini N, Botez RM, Ceruti A, Wong T. Optimization and Design of a Flexible Droop Nose Leading Edge Morphing Wing Based on a Novel Black Widow Optimization (B.W.O.) Algorithm—Part II. Designs. 2022; 6(6):102. https://doi.org/10.3390/designs6060102

[10] Beyeler, A., Zufferey, JC and Floreano, D. Vision-based control of near-obstacle flight. Auton Robot 27, 201–219 (2009). https://doi.org/10.1007/s10514-009-9139-6

[11] Barry, AJ, Florence, PR, Tedrake, R. High-speed autonomous obstacle avoidance with pushbroom stereo. J Field Robotics. 2018; 35: 52–68. https://doi.org/10.1002/rob.21741

[12] E. Bulka and M. Nahon, "High-Speed Obstacle-Avoidance with Agile Fixed-Wing Aircraft," 2019 International Conference on Unmanned Aircraft Systems (ICUAS), Atlanta, GA, USA, 2019, pp. 971-980, doi: 10.1109/ICUAS.2019.8797720.

[13] S. Keshmiri, A. R. Kim, D. Shukla, A. Blevins and M. Ewing, "Flight Test Validation of Collision and Obstacle Avoidance in Fixed-Wing UASs with High Speeds Using Morphing Potential Field," 2018 International Conference on Unmanned Aircraft Systems (ICUAS), Dallas, TX, USA, 2018, pp. 589-598, doi: 10.1109/ICUAS.2018.8453299.

[14] Online Feasible Trajectory Generation for Collision Avoidance in Fixed-Wing Unmanned Aerial Vehicles Min Prasad Adhikari and Anton H. J. de Ruiter Journal of Guidance, Control, and Dynamics 2020 43:6, 1201-1209

[15] Mirzaee Kahagh, A., Pazooki, F., Etemadi Haghighi, S., and Asadi, D. (2022). Real-time formation control and obstacle avoidance algorithm for fixed-wing UAVs. The Aeronautical Journal, 126(1306), 2111-2133. doi:10.1017/aer.2022.9

[16] Lin, Z., Castano, L., Mortimer, E. et al. Fast 3D Collision Avoidance Algorithm for Fixed Wing UAS. J Intell Robot Syst 97, 577–604 (2020). https://doi.org/10.1007/s10846-019-01037-7

[17] N. J. Sanket, C. D. Singh, K. Ganguly, C. Fermüller and Y. Aloimonos, "GapFlyt: Active Vision Based Minimalist Structure-Less Gap Detection For Quadrotor Flight," in IEEE Robotics and Automation Letters, vol. 3, no. 4, pp. 2799-2806, Oct. 2018, doi: 10.1109/LRA.2018.2843445.

[18] S. Jiang, K. A. Stol, W. Xu and B. Graham, "Towards autonomous flight of an unmanned aerial system in plantation forests," 2016 International Conference on Unmanned Aircraft Systems (ICUAS), Arlington, VA, USA, 2016, pp. 911-919, doi: 10.1109/ICUAS.2016.7502613.

[19] Zhao, N., Luo, Y., Deng, H., and Shen, Y. (June 18, 2018). "The Deformable Quad-Rotor: Mechanism Design, Kinematics, and Dynamics Effects Investigation." ASME. J. Mechanisms Robotics. August 2018; 10(4): 045002. https://doi.org/10.1115/1.4040355

[20] A. J. Barry et al., "Flying between obstacles with an autonomous knife-edge maneuver," 2014 IEEE International Conference on Robotics and Automation (ICRA), Hong Kong, China, 2014, pp. 2559-2559, doi: 10.1109/ICRA.2014.6907217.